Journal of Materials Chemistry A

High Thermoelectric Performance in Complex Phosphides Enabled by Stereochemically Active Lone Pair Electrons

Journal:	*Journal of Materials Chemistry A*
Manuscript ID	TA-ART-08-2018-008448.R2
Article Type:	Paper
Date Submitted by the Author:	20-Nov-2018

Complete List of Authors:	Shen, Xingchen; Chongqing University; Chinese Academy of Science, Chongqing Institute of Green and Intelligent Technology; China and University of Chinese Academy of Sciences Xia, Yi; Center for Nanoscale Materials, Argonne National Laboratory Wang, Guiwen; Chongqing University, Zhou, Fei; LLNL, Ozolins, Vidvuds; Department of Applied Physics, Yale University Lu, Xu; Chongqing University, College of Physics Wang, Guoyu; Chinese Academy of Sciences, Chongqing Institute of Green and Intelligent Technology Zhou, Xiaoyuan; Chongqing University,

Journal Name

ARTICLE

High Thermoelectric Performance in Complex Phosphides Enabled by Stereochemically Active Lone Pair Electrons

Xingchen Shen,‡[af] Yi Xia,‡[b] Guiwen Wang,[c] Fei Zhou,[d] Vidvuds Ozolins,[e] Xu Lu,*[a] Guoyu Wang,*[f] Xiaoyuan Zhou*[ac]

Received 00th January 20xx,
Accepted 00th January 20xx

DOI: 10.1039/x0xx00000x

www.rsc.org/

We propose a new strategy to design high performance thermoelectric materials with stereochemically active lone pair electrons. This novel concept is experimentally demonstrated in the cluster compounds $Ag_6Ge_{10(1-x)}Ga_{10x}P_{12}$ with x = 0.0, 0.01, 0.03, 0.04. A maximum power factor of 13 μW cm^{-1} K^{-2} is achieved after optimizing carrier concentration. Density funcitonal theory calculations reveal that the stereochemically active lone pair electrons from s orbitals of Ge give rise to a peak in the density of states near the valence band maximum, a feature that is benefical for achieving high power factor. Experimental results also confirm the theoretically predicted relatively low thermal conductivity of about 1 W m^{-1} K^{-1} arising from the rattling vibrations associated with Ag_6 clusters, which create low-frequency localized optical phonons in the acoustic region and thus enable strong anharmonic phonon scattering. The highest zT value attained here is 0.65 at 723 K for the x = 0.03 sample, a record high value for polycrystalline phosphide and still with significant potential for optimization.

1. Introduction

Many efforts have been devoted to searching for new thermoelectric (TE) materials with high efficiency, which could be used in waste heat recovery by directly converting heat into electricity.[1-2] The performance of TE materials is characterized by the dimensionless figure of merit $zT=S^2\sigma T/\kappa$, where S is the Seebeck coefficient, σ is the electrical conductivity, T is the absolute temperature, and κ is the thermal conductivity. $S^2\sigma$ is termed as power factor, which determines the capability of power output of TE materials. The maximum value of power factor for certain compounds is principally governed by their intrinsic band structure and doping solubility. As for the thermal conductivity κ, which consists of electronic and lattice contribution, the most commonly used method for its reduction relies on lowering the lattice part. When moving to the device or system level, the practical viability of large-scale TE generators requires materials with both high zT and earth-abundance of their constituent elements. However, in most thermoelectrics the constituent anions are Te, Se or Sb, all of which are relatively scarce. These heavy elements are believed to be the key to attaining low lattice thermal conductivity, which generally decreases with increasing atomic weight.[3] Phosphides would be attractive as TE materials since P is at least three orders of magnitude more earth-abundant than the aforementioned elements. However, phosphides are usually ignored by most of the thermoelectric research community, and only a few studies of the thermoelectric properties of phosphides have been reported.[4-6] The main obstacle for the development of phosphide based thermoelectrics originates from their limited power factor, mostly due to their unfavorable band structure. In

[a] Chongqing Key Laboratory of Soft Condensed Matter Physics and Smart Materials，College of Physics, Chongqing University, Chongqing, Chongqing 401331, P. R. China. Email: luxu@cqu.edu.cn; xiaoyuan2013@cqu.edu.cn
[b] Department of Materials Science and Engineering, Northwestern University, Evanston, IL 60208, USA
[c] . Analytical and Testing Center of Chongqing University, Chongqing 401331, P. R. China
[d] Physical and Life Sciences Directorate, Lawrence Livermore National Laboratory, California 94550, USA
[e] Department of Applied Physics, Yale University, New Haven, Connecticut 06511, USA, and Energy Sciences Institute, Yale University, West Haven, Connecticut 06516, USA
[f] Chongqing Institute of Green and Intelligent Technology, Chinese Academy of Sciences Chongqing 400714, P. R. China and University of Chinese Academy of Sciences, Beijing, 100044, P. R. China. Email: guoyuw@cigit.ac.cn;
† Electronic Supplementary Information (ESI) available: See DOI: 10.1039/x0xx00000x
‡ X. S and Y. X contributed equally to this work.

addition, the relatively high lattice thermal conductivity further hinders the realization of high *zT* in phosphides. Therefore, searching for phosphides with favorable band features and low lattice thermal conductivity becomes imperative.

Mahan and Sofo theoretically manifested that the optimum shape of band extrema for materials with high power factor should contain a sharp onset of sharply rising density of states near band edges.[7] Such scenario can be realized in quantum well structures, in which Fermi surfaces take the shape of plate or sheet rather than the sphere or ellipsoids for traditional three-dimensional bulk solids.[8] However, the difficulty in fabrication of high quality superlattice and the potential strong scattering for carriers among interfaces impede the development of TE devices based on superlattice. The contradiction was partly resolved by utilizing localized d/f electron orbitals in some transition metal or rare earth elements in the certain intermetallic compounds below room temperature.[9] Most recently, Parker et al. demonstrated that low-dimensional bands can be realized in bulk materials enabled by carrier pocket anisotropy even in compounds with cubic structure.[10-11] Bilc et al. theoretically extended such idea to boost power factor in some semiconducting Heusler compounds by exploiting the highly directional d orbitals of Fe atoms.[12] Herein, we first present a new approach to create the peaks in density of states (DOS) near band edges by utilizing stereochemically active lone pair electrons instead of the d/f orbitals in metal elements, as demonstrated experimentally by the case of $Ag_6Ge_{10}P_{12}$ phosphide compounds. We noticed that the synthesis and thermoelectric performance of pristine single and polycrystalline$Ag_6Ge_{10}P_{12}$ have been reported very recently.[13] From a largely different perspective, we focus on the validation of the purposed novel strategy in the heavily hole-doped $Ag_6Ge_{10}P_{12}$ compounds with unique plate-like band feature. For this purpose, we have experimentally synthesized and investigated the thermoelectric properties of pristine and Ga-doped $Ag_6Ge_{10(1-x)}Ga_{10x}P_{12}$ compounds with *x* ranging from 0.0 to 0.04. It is found that these compounds can achieve an extraordinarily large power factor of 10.5-13 μW cm^{-1} K^{-2} over the entire measured temperature region after proper doping, very promising for practical application. Our first-principles density-functional theory (DFT) calculations reveal that $Ag_6Ge_{10}P_{12}$ compounds possess a characteristic plate-like hole pocket feature with highly anisotropic (light and heavy) effective masses, which is derived from the stereochemically active lone pair electrons in constituent Ge atoms. Furthermore, the measured lattice thermal conductivity of these compounds decreases to 1 W m^{-1} K^{-1} at high temperature, which is an unusually low value among phosphide compounds. We ascribe the intrinsically low lattice thermal conductivity to the strong anharmonic scattering associated with rattling motions of the Ag_6 cluster, evidenced by our first-principles calculations based on a newly developed compressive sensing lattice dynamics (CSLD) method.[14] Finally, the maximum *zT* value of 0.65 is attained for $x = 0.03$ sample at 723 K, a record high value for polycrystalline phosphide compounds. Our results not only demonstrate that phosphides can be good thermoelectrics but also a new avenue for searching for new TE materials with plate-like carrier pocket induced by the lone pair electrons that contribute to the band extrema.

2. Experimental section

2.1 Synthesis

Polycrystalline samples of composition $Ag_6Ge_{10(1-x)}Ga_{10x}P_{12}$ ($x = 0.0, 0.01, 0.03, 0.04$) were synthesized by the conventional solid state reaction and annealing procedure. Stoichiometric amounts of high purity elemental Ag (granular, 99.999%), Ge (pieces, 99.999%), Ga (pieces, 99.999%) are mixed with a 10% excess of red phosphorus–P (99.999%, bulk) followed by putting into fused quartz tubes. The excess P is proved to be crucial to form $Ag_6Ge_{10}P_{12}$ phase both by previous studies and our experimental trials in that volatile character of P inevitably causes loss of P during the heating process. Subsequently, all the tubes were evacuated to 10^{-4} Pa, and then quickly were sealed. Thereafter, the tubes were put into the muffle furnace, slowly heated from room temperature to 1323 K in 60 hours. Then those tubes were kept at this temperature for 3 days and then slowly cooled down to room temperature in 48 hours. The obtained ingots were reground into fine powders and annealed for 3 days, and then left to a natural cooling. The annealed fine powders were consolidated by Spark Plasma Sintering (SPS) at 873 K for 5 minutes under the pressure of 45 MPa in an Ar-flow atmosphere. The final products were confirmed

to have 95% of theoretical density by using the Archimedes method.

2.2 Characterization

The high temperature electrical properties including the electrical resistivity (σ) and Seebeck coefficient (S) were measured by Linseis LSR-3 system, while the thermal conductivity was calculated from the formula $\kappa = \lambda C_p \rho$, where the thermal diffusivity (λ) was obtained using Netzsch LFA 457 lasher flash system, and the heat capacity (Cp) value was measured using a differential scanning calorimeter (DSC) apparatus (Netzsch, 404 F3). We estimate that the uncertainties in our electrical and thermal transport measurements are 5% and 10%, respectively. Powder x-ray diffraction (XRD) patterns of all samples after SPS were collected using a PANalytical X'Pert apparatus with Cu κ_α radiation. The data was analyzed by the commercial software JADE 8.0. The microstructure and composition analyses were measured using field emission scanning electron microscopy (SEM, JSM-7800F, JEOL) equipped with an energy dispersive spectrometer (EDS). The chemical valence states of all the elements were determined on X-ray Photoelectron Spectroscopy (XPS, ESCALAB250Xi, ThermoFisher Scientific) using Mg κ_α as the excitation source.

2.3 Calculation

Density-functional theory (DFT) calculations were performed with the projector-augmented wave (PAW)[15] method as implemented in the Vienna Ab initio Simulation package (VASP).[16-17] The structure was fully relaxed using a Brillouin zone origin-centered 6×6×6 k-point mesh and a plane wave cutoff energy of 520 eV. The Perdew-Becke-Ernzerhof revised for solids (PBEsol)[18-19] exchange-correlation (xc) functional was used to perform structure relaxation and band structure calculations. Electronic density-of-states (DOS) was calculated using a 30×30×30 k-point mesh. Both second- and third-order interatomic force constants (IFCs) were computed using the compressive sensing lattice dynamics (CSLD) method.[20] Supercell structures each containing 448 atoms with random small atomic displacements were used as training data to fit IFCs. Phonon dispersion curves were calculated using second–order IFCs. Phonon mode-resolved lifetimes and lattice thermal conductivity were calculated using third-order IFCs by taking into account anharmonic three-phonon scattering processes theory within Boltzmann transport equation (BTE) as implemented in the ShengBTE package.[21]

3. Results and discussion

3.1 Phase and valence state analysis

$Ag_6Ge_{10}P_{12}$, the first member of a family of cluster compounds, bears a structural resemblance to the tetrahedrite $Cu_{12}Sb_4S_{13}$, which has been intensively studied as earth-abundant TE materials recently,[22-25] in the ($I\bar{4}3m$) space group with a = 10.268 Å. According to symmetry, all Ag and P atoms are symmetrically equivalent, while Ge atoms occupy two different sites, indicated by Ge(1) and Ge(2), which are bonded to three P atoms and four P atoms, respectively. As shown in Fig. 1, the structure can be most easily interpreted as an assembly of $Ag_6Ge(1)_4P_{12}$ clusters, which are interconnected by the remaining Ge(2) atoms. An octahedral cluster composed of six Ag atoms with its eight triangular faces capped by Ge(1) atoms is formed at the center of each $Ag_6Ge(1)_4P_{12}$ cluster. By a simple valence counting rule, the Ag_6 cluster takes 4^+ valence state as a whole, while Ge(1) atoms exhibit 2^+ state, leaving a lone pair of electrons (shown in Fig. 1(c)). It is also found that Ag_6 octahedral cluster is rather weakly coupled to surrounding network of covalent bonds formed by Ge and P atoms. The crystal structure is further completed with two P atoms near each Ag atoms. Fig. 1(d) displays the room temperature X-ray diffraction patterns of the bulk samples $Ag_6Ge_{10(1-x)}Ga_{10x}P_{12}$ (x = 0.0, 0.01, 0.03, 0.04). Most of the peaks can be indexed well with the standard card of $Ag_6Ge_{10}P_{12}$ phase (PDF #80-2192, No. 217). However, a minute portion of Ge second phase appears in the patterns, which is marked with black rhombi, even though a 10% excess of red phosphorus has been added. The thermal stability of pristine $Ag_6Ge_{10}P_{12}$ was checked by high temperature differential scanning calorimetry (DSC) measurement from room temperature to 923 K. We observed that the decomposition of the sample begins at 750 K probably due to the loss of volatile P, which is implied by the rapid drop in heat capacity (shown in Fig. S1). Herein, the thermoelectric property measurements were made below 723 K. Fig. S2(a, b) shows the SEM-EDX mapping analysis of the fracture surface of $Ag_6Ge_{9.7}Ga_{0.3}P_{12}$, which confirms that all the elements (Ag, Ge, P, Ga) appear and distribute homogeneously throughout the sample.

Specifically, it is noted that the average atomic percentage of the doping element Ga is 0.8%, which is close to the nominal Ga doping percentage of 1.1%. To identify the actual valence state of all the elements in these complex phosphide compounds as claimed by the valence counting rule, XPS measurement was carried out on the representative sample $Ag_6Ge_{9.7}Ga_{0.3}P_{12}$ and the results are shown in Fig. 2. As displayed in Fig. 2(c), in the higher binding energy region, the characteristic peaks of Ge 3d are found at 31.2 eV and 32.6 eV, indicating the coexistence of Ge^{2+} and Ge^{4+} valence state and an assured appearance of lone pair electrons in this compound. Meanwhile, the elemental Ge peak appears in the lower binding energy region,

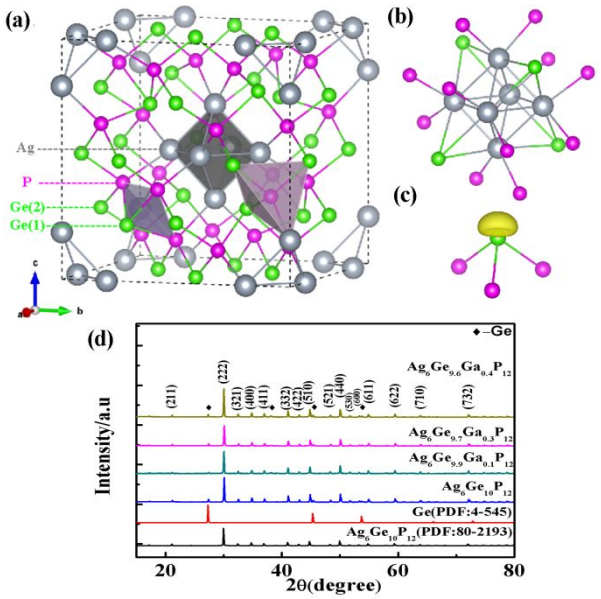

Fig. 1. (a) Crystal structure of $Ag_6Ge_{10}P_{12}$ (gray: Ag; green: Ge; magenta: P); (b) Central $Ag_6Ge(1)_4P_{12}$ cluster; (c) Charge density of the highest occupied valence band showing the lone pair electrons on Ge(1) atoms; (d) XRD patterns of $Ag_6Ge_{10(1-x)}Ga_{10x}P_{12}$ (x = 0.0, 0.01, 0.03, 0.04).

further confirming the existence of Ge secondary phase found in XRD patterns. More importantly, in order to substantiate the successful Ga-doping, the XPS spectrum of Ga of $Ag_6Ge_{9.7}Ga_{0.3}P_{12}$ is shown in Fig. 2(e). The Ga 2p spectrum splits into $2p_{1/2}$ and $2p_{3/2}$ components at the binding energy of 1117.5 eV and 1144.9 eV respectively, as shown in Fig. 2(e). Similar spectrum of Ga^{3+} state has been reported before in $AgGaS_2$ compound.[26] Since no peaks can be identified for elemental Ga in the measurement, we certainly can claim that most Ga exist as Ga^{3+} in the sample.

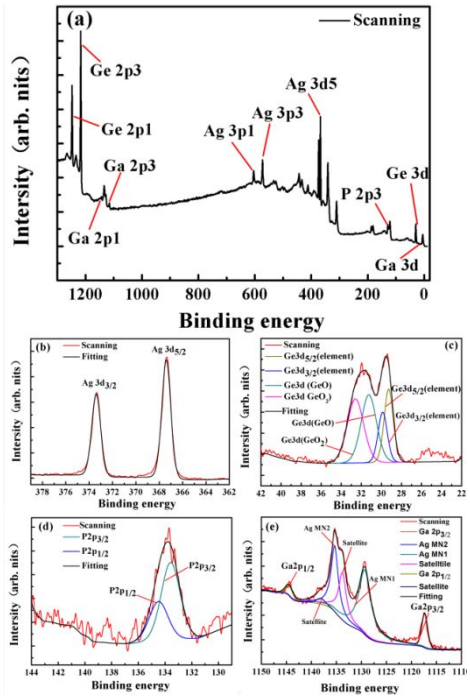

Fig. 2. (a) XPS full spectra of the fractured surface of $Ag_6Ge_{9.7}Ga_{0.3}P_{12}$ (b) Fitted spectra of Ag 3*d*, Ge 3*d* (c), P 2*p* (d), Ga 2*p* (e) for fractured surface of $Ag_6Ge_{9.7}Ga_{0.3}P_{12}$.

3.2 Electrical transport and band structure of $Ag_6Ge_{10}P_{12}$

The experimental electrical transport properties are displayed in Fig. 3. Fig. 3(a) shows the electrical resistivity of $Ag_6Ge10_{(1-x)}Ga_{10x}P_{12}$ with x ranging from 0 to 0.04. For pristine and x = 0.01 sample, the resistivity decreases with increasing temperature, clearly showing an activation mechanism for hole transport below 500 K. At higher temperature, the resistivity of these two samples increases with temperature due to the saturated carrier concentration and diminished mobility. In contrast, the x = 0.03 and 0.04 samples exhibit a typical highly degenerate semiconductor behavior, where the resistivity increases continuously with temperature. Meanwhile, the resistivity drops significantly with increasing Ga content in the whole measured temperature range, indicating an increased carrier concentration via successful p-type doping by Ga. The room-temperature carrier concentration along with the electrical transport property is listed in Table 1. All the Ga doped samples show the carrier concentration on the order of 10^{20}~10^{21} cm^{-3} compared with that of 10^{19} cm^{-3} of the pristine compound $Ag_6Ge_{10}P_{12}$, suggesting that

Ga doping is effective in tuning the carrier concentration and thus leads to the significantly enhanced electrical conductivity. Compared to the pristine sample with resistivity on the order of 10 mΩ cm, the resistivity of heavily doped samples (x = 0.03 and 0.04) is on the order of 1 mΩ cm, comparable to other good thermoelectric materials. Moving now to the Seebeck coefficient (Fig. 3(b)), the Seebeck coefficients of all samples are positive, implying that the majority carriers in these compounds are holes; the values increase monotonously with respect to temperature up to the highest measured temperature and no bipolar effect is observed. With increasing Ga content, the Seebeck coefficients diminish, following the general trend given by $S \propto (1/n)^{2/3}$, where n is carrier concentration. The maximum PF of $Ag_6Ge_{9.7}Ga_{0.3}P_{12}$ reaches 13 $\mu Wcm^{-1}K^{-2}$, which is the highest PF value obtained hitherto for polycrystalline phosphides (shown in Fig. 3).[4-6] More interestingly, it is also noted that the PF of the optimum sample varies slightly with respect to temperature and is well maintained above 10.5 $\mu Wcm^{-1}K^{-2}$ from room temperature to highest measured temperature, which is comparable to the PFs for the best p-type TE materials on average.[27-32]

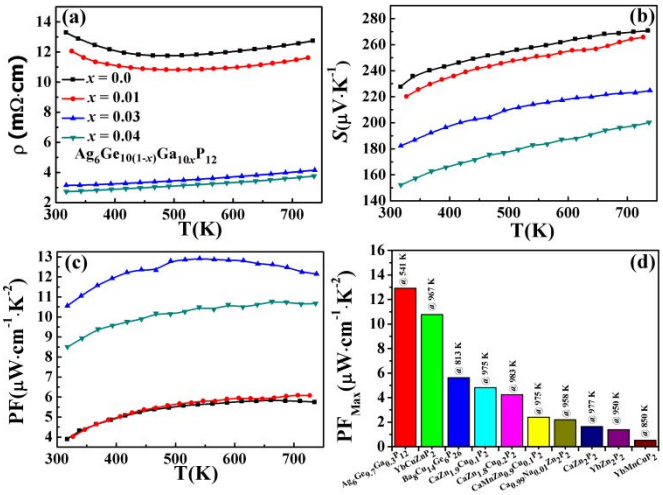

Fig. 3. (a) Temperature dependence of the electrical resistivity for $Ag_6Ge_{10(1-x)}Ga_{10x}P_{12}$ (x = 0.0, 0.01, 0.03, 0.04); (b) Temperature dependence of the Seebeck coefficient for $Ag_6Ge_{10(1-x)}Ga_{10x}P_{12}$($x$ = 0.0, 0.01, 0.03, 0.04); (c) Temperature dependence of the power factor for $Ag_6Ge_{10(1-x)}Ga_{10x}P_{12}$($x$ = 0.0, 0.01, 0.03, 0.04); (d) The maximum power factor of $Ag_6Ge_{10(1-x)}Ga_{10x}P_{12}$($x$ = 0.03), $Ba_8Cu_{14}Ge_6P_{26}$,[4] Zintl polycrystalline phosphides $AMXP_2$. [5-6]

For the purpose of understanding the superior electrical transport performance, we performed DFT calculation

Table 1. Carrier concentration (n), electrical conductivity (σ), Seebeck coefficient (S), power factor (PF) for all the $Ag_6Ge_{10(1-x)}Ga_{10x}P_{12}$ samples at room temperature.

Composition	n (cm^{-3})	σ ($S{\cdot}m^{-1}$)	S ($\mu V{\cdot}K^{-1}$)	PF ($\mu W{\cdot}cm^{-1}{\cdot}K^{-2}$)
x = 0.0	6.18E+19	7522	228	3.9
x = 0.01	1.44E+20	8294	220	4.0
x = 0.03	2.41E+21	31773	182	10.6
x = 0.04	1.32E+21	36725	152	8.5

for the electronic structure of $Ag_6Ge_{10}P_{12}$. Previously, $Ag_6Ge_{10}P_{12}$ was considered as a p-type semiconductor with a fully filled valence band and a band gap of 0.76 eV at room temperature, as reported by Bullett and Witchlow.[33-34] Our calculated DFT band structure in Fig. 4(a) suggests that $Ag_6Ge_{10}P_{12}$ is a semiconductor with an indirect band gap of approximately 0.45 eV, where the VBM and CBM occur along the P-H and Γ-H lines, respectively. The details of high symmetry points in Brillouin zone can be found in Fig. S3. Our computed band gap appears to be underestimated in comparison with the experimental measurement due to a well-known shortcoming of approximate DFT functionals.[35] Considering the p-type conducting nature of this compound, we focus on the profile of VBM, which is located along P-H (Λ) line. This carrier pocket is highly anisotropic that it is dispersive when viewed along P-H line while rather flat along Σ-Λ direction, which we term as "plate-like" behavior (Fig. 4(b)). In addition, the very large effective mass associated with the flat dispersionless portion along the Σ-Λ path leads to connected Fermi surface rings. Fig. 4(b) and Fig. S3(b) show the Fermi surface of hole-doped $Ag_6Ge_{10}P_{12}$ with the Fermi level at 50 meV below the VBM, wherein the hole pockets have merged into six anisotropic rings that encircle the Γ-H lines. Furthermore, there are multiple hole pockets along the Γ-H (Δ), H-N (Σ), and P-H (Λ) lines in the (a). As demonstrated by previous studies,[33-34] $Ag_6Ge_{10}P_{12}$ is a valence precise compound, of which the semiconducting band gap can be understood by counting electrons, wherein Ge(2) and P atoms are in normal Ge^{4+} and P^{3-} states respectively, while Ge(1)

atoms are in Ge^{2+} state with an unoccupied lone pair electron pointing toward one of the triangular faces of the Ag_6^{4+} clusters, implying a highly directional charge density distribution. This subvalency associated with Ag_6 clusters, which exhibits mixed valence state for Ag atoms between Ag^{0+} and Ag^{1+}, has been confirmed by spectroscopic evidence and attributed to the closeness in energy between Fermi level and Ag empty 5s orbitals.[39] Unlike ternary metal chalcogen compounds, the metal Ag here has relatively small contribution to the band edges since Ag_6 cluster is somewhat independent from the main framework associated with weak chemical bonding between the environment. Instead, the Ge(1) atoms take the role of main cation and thus the lone pair electrons are capable of contributing to the band edges. Indeed, as can be seen from Fig. 5(a)-(b), the VBM is mainly composed of Ag d, P p and Ge(1) s orbitals, indicating a complex hybridization between these orbitals and these lone pair electrons are stereochemically active rather than inert as typically thought. Further comparison between Ge(1) and Ge(2) reveals the presence of sharp DOS peak associated with lone pair electrons in the vicinity of VBM on Ge(1) sites. The plotted charge density of the highest occupied valence band, as shown in Fig. 4(c), clearly displays the stereochemically active lone pair electrons on Ge(1) atoms and subvalence electron in Ag_6 cluster.

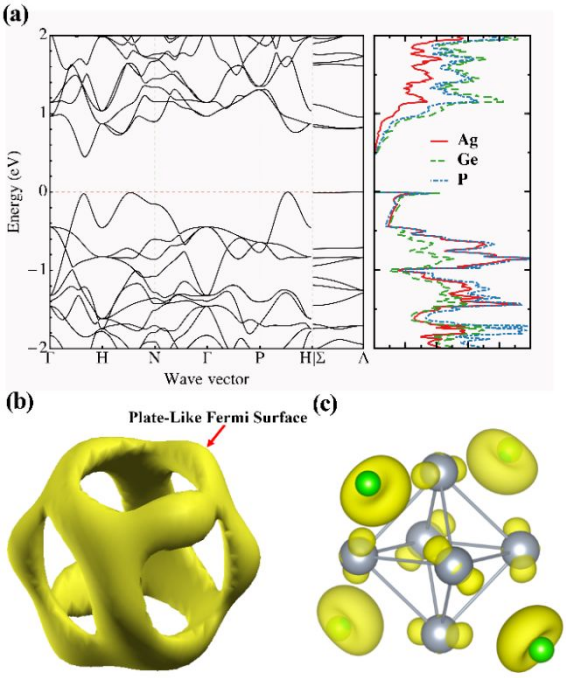

Fig. 4. (a) Band structure of $Ag_6Ge_{10}P_{12}$; (b) Fermi surface of hole carriers for the Fermi level set at 50 meV below the VBM; (c) Charge density of the highest occupied valence band showing localized orbitals associated with Ge(1) and Ag atoms.

Eventually, we are able to verify that the lone pair electrons from Ge(1) is responsible for plate-like carrier pocket and superior electrical transport properties. We also investigated the effects of Ga doping by substituting one Ge atom with Ga atom in a primitive cell. The DFT total energy shows that Ga tends to occupy Ge(2) site, which has an energy of about 0.05 eV per formula unit lower than Ge(1) site. For both cases, the resulting band structure and density of states (see Fig. S4) clearly show that the Fermi level moves into the valence band, further supporting the experimentally observed increased hole concentration via Ga doping. It is noted that the maximum PF of $Ag_6Ge_{10}P_{12}$ is comparable but still lower than that for mainstream TE materials due to the difficulty in controlling the doping content in phosphides and the relatively low decomposition temperature. Higher PF is expected if more accurate doping can be performed and or the loss of P can be effectively prevented at high temperature.

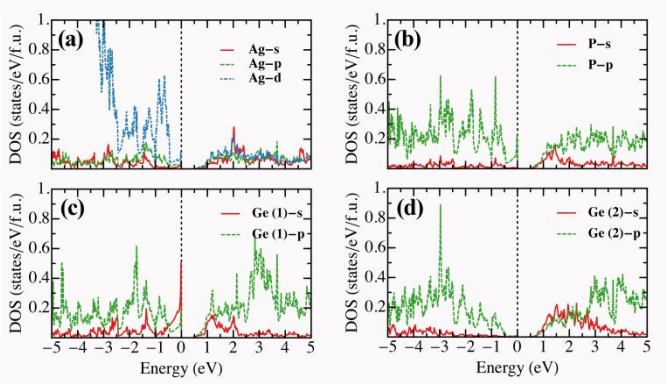

Fig. 5. (a)-(d) Atom-decomposed density of states of $Ag_6Ge_{10}P_{12}$. The vertical black dashed lines indicate the VBM.

3.3 Thermal transport properties and phonon modes of $Ag_6Ge_{10}P_{12}$

Fig. 6(a) displays the total thermal conductivity measured from room temperature to 723 K. We see that the thermal conductivity is between 2.3 W m^{-1} K^{-1} and 1.2 W m^{-1} K^{-1} over the entire temperature range. The thermal conductivity increases monotonically with increasing Ga content due to the increased electronic part of thermal conductivity. The Wiedemann-Franz law with a constant Lorenz number of the free electron

value is applied to estimate the electronic contribution of thermal conductivity. After subtracting the electronic part, we obtain the lattice thermal conductivity and the result is shown in Fig. 6(b). All the lattice thermal conductivity follows the T^{-1} rule, indicating the Umklapp phonon-phonon interaction dominates in those compounds. At 723 K, all the samples possess a lattice thermal conductivity around 1.0~1.1 W m^{-1} K^{-1}, which is a relatively low value compared with other phosphide compounds.[4-6,40]

Intrinsically low lattice thermal conductivity is fundamentally important to achieve high *zT*, which motivates us to investigate lattice heat transport in phosphide compounds. Fig. 7(a)-(b) shows the calculated phonon dispersions and atom-projected density of states of $Ag_6Ge_{10}P_{12}$. Unlike $Cu_{12}Sb_4S_{13}$, which exhibits unstable optical modes,[37] phonon modes of $Ag_6Ge_{10}P_{12}$ are all dynamically stable. However, both compounds share prominent feature of the presence of low-lying rattling modes, cutting through the acoustic region. For $Ag_6Ge_{10}P_{12}$, acoustic modes are flattened near 6 meV towards the edge of Brillouin zone, and nearly flat low-energy (4 meV) optical phonon modes are found in the acoustic region, both of which are mostly associated with vibrations of Ag atoms. These flat phonon modes with approximately zero group velocity reflect the locality of vibrations of Ag atoms and confirm the weakness of covalent bonding between Ag_6 cluster and surroundings. In addition to reducing group velocities, these localized modes act as scattering centers for low-energy acoustic modes, referred as resonant scattering,[20] thus further reducing total lattice thermal conductivity. Aiming at further verifying the calculated phonon dispersion, we preformed the low temperature heat capacity measurement for $Ag_6Ge_{10}P_{12}$ and the result is shown in Fig. 7(c). As is well known, the low temperature heat capacity is relevant to the lattice vibration modes, which determines the intrinsic lattice thermal conductivity. Theoretically, we calculated the constant volume heat capacity based on the following formula,

$$C_V = \sum_{qv} k_B \left(\frac{\hbar\omega_{qv}}{k_B T}\right)^2 \frac{\exp(\hbar\omega_{qv}/k_B T)}{\left(\exp\left(\frac{\hbar\omega_{qv}}{k_B T}\right)-1\right)^2}$$

where q, v, ω are phonon waver vector, branch index and frequency, respectively. The above parameters were obtained from regular phonon dispersion calculations. Fig. 7(c) compares our theoretically calculated heat capacity with experimental measurement.

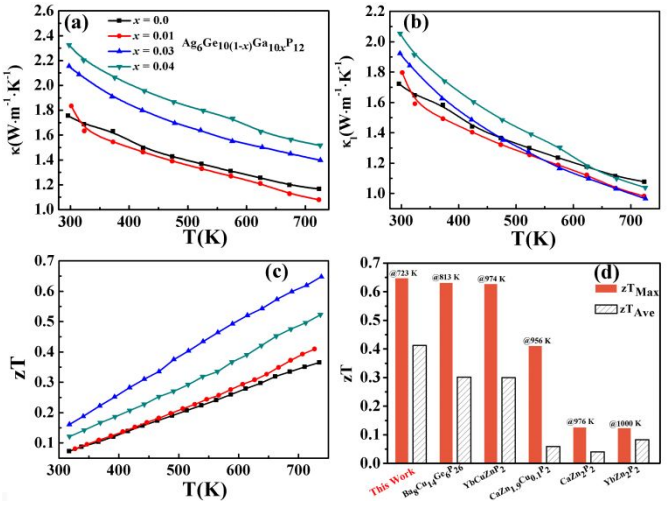

Fig. 6. (a) Temperature dependence of the total thermal conductivity κ for $Ag_6Ge_{10(1-x)}Ga_{10x}P_{12}$($x$ = 0.0, 0.01, 0.03, 0.04); (b) Temperature dependence of the lattice conductivity κ_L for $Ag_6Ge_{10(1-x)}Ga_{10x}P_{12}$($x$ = 0.0, 0.01, 0.03, 0.04); (c) Temperature dependence of the *zT* values for $Ag_6Ge_{10(1-x)}Ga_{10x}P_{12}$($x$ = 0.0, 0.01, 0.03, 0.04); (d) The maximum and average *zT* values of $Ag_6Ge_{9.7}Ga_{0.3}P_{12}$, $Ba_8Cu_{14}Ge_6P_{26}$, [4] Zintl polycrystalline phosphides $AMXP_2$. [5-6]

The good agreement below 200 K further verifies our calculated phonon dispersion, while the deviation at higher temperature is possibly due to the anharmonic effects, such as thermal expansion and anharmonic frequency shift. To quantitatively access the lattice thermal conductivity, we used the recently developed compressive sensing lattice dynamics (CSLD) method[20] within the theoretical framework of anharmonic lattice dynamics and Boltzmann transport equation (BTE).[41] Anharmonic interatomic force constants (IFCs) were extracted and utilized to estimate the phonon scattering rates considering three-phonon processes. Fig. S5(a)-(b) show the calculated phonon mode group velocity and lifetime. Both group velocity and lifetime are drastically reduced around the flat phonon bands, confirming the presence of resonant scattering. The computed lattice thermal conductivity is shown in Fig. 7(d). $Ag_6Ge_{10}P_{12}$ has a low lattice thermal conductivity of about 1.2 W m^{-1} K^{-1} at 300 K and further decreases to 0.5 W m^{-1} K^{-1} at 700 K, comparable to $Cu_{12}Sb_4S_{13}$. Our predicted lattice thermal conductivity is lower than experimental

measurement which probably could be attributed to (1) the presence of pure Ge phase which has much larger lattice thermal conductivity in experimental samples; (2) the neglect of temperature induced renormalization of phonon dispersions and third-order IFCs; and (3) underestimation of phonon mean free path in BTE which falls below interatomic distance. Considering the relatively small deviation of the measured thermal conductivity from the predicted one, we conclude that the observed low thermal conductivity of $Ag_6Ge_{10}P_{12}$ compounds can be majorly ascribed to the local vibrational modes associated with Ag_6 cluster, which induce strong anharmonic phonon-phonon interactions. The fact that measured thermal conductivity of $Ag_6Ge_{10(1-x)}Ga_{10x}P_{12}$ compounds is still higher than that predicted by theoretical calculation motivates further investigations regarding getting rid of residual Ge, which could further enhance *zT*.

3.4 Thermoelectric properties of $Ag_6Ge_{10}P_{12}$

By combining the electronical transport and thermal conductivity data, the overall figure of merit (*zT*) values are calculated and shown in Fig. 6(c). The pure $Ag_6Ge_{10}P_{12}$ sample exhibits a *zT* value of 0.3 while $Ag_6Ge_{9.7}Ga_{0.3}P_{12}$ sample shows a *zT* value of 0.65, a record high value for polycrystalline phosphides (Fig. 6(d)), resulting from optimized carrier concentration, namely the position of Fermi level. Since the *zT* values of all samples increase linearly with respect to temperature, the average *zT* of $Ag_6Ge_{9.7}Ga_{0.3}P_{12}$ sample is close to 0.4 from room temperature to 723 K, which is another overwhelming advantage compared to other phosphides.[4-6]

4. Conclusions

We present a new route to satisfy the criteria for best thermoelectrics by utilizing the stereochemically active lone pair electrons to highly directional electronic states. The concept is successful realized in the novel phosphide compounds $Ag_6Ge_{10}P_{12}$, which exhibit excellent electrical performance with PF maintained in the range of 10.5-13 μW cm^{-1} K^{-2} from room temperature to high temperature after optimizing carrier concentration. A highly anisotropic plate-like carrier pocket, mainly resulting from the directional lone pair electrons is identified by theoretical calculation. In addition, the relatively low lattice thermal conductivity

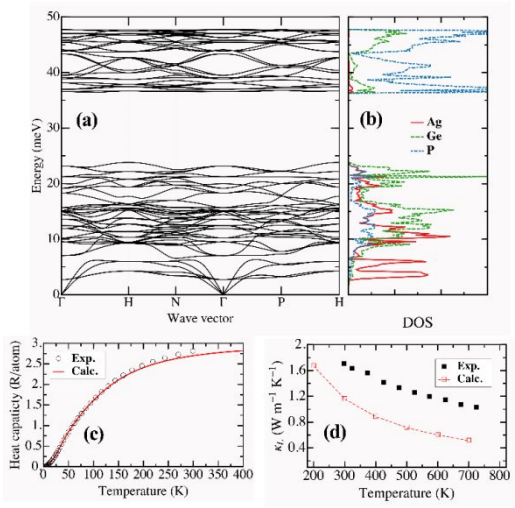

Fig. 7. (a) Phonon dispersions of $Ag_6Ge_{10}P_{12}$; (b) Atom-projected phonon density of states; (c) Computed heat capacity compared with experimental measurement; (d) Computed lattice thermal conductivity compared with experimental measurement.

around 1 W m^{-1} K^{-1} is attained at high temperature. The analysis based on the specific heat data and theoretical lattice thermodynamic calculation substantiates the existence of strong anharmonicity caused by the local vibrational modes of Ag_6 cluster, yielding the low thermal conductivity. The relatively low lattice thermal conductivity and favorable PF give birth to a maximum *zT* value of 0.65, which is a record high value for polycrystalline phosphide compounds. The complex electronic band structure and various choices of doping elements leave much scope of continuing work to further enhance the PF and reduce lattice thermal conductivity for $Ag_6Ge_{10}P_{12}$ based compounds. In all, our study demonstrates that phosphorus, which is among the most earth-abundant elements, can serve as main anion for thermoelectric semiconductors. More importantly, taking this study as an example, our proposed new avenue for searching for good thermoelectrics in the compounds with stereochemically active lone pair electrons is practicable.

Conflicts of interest

The authors declare no competing financial interest.

Acknowledgements

This work was financially supported in part by the National Natural Science Foundation of China (Grant

Nos. 51772035, 11674040, 51672270), the Fundamental Research Funds for the Central Universities (106112017CDJQJ308821 and 106112016CDJZR308808). XCS appreciated the Fundamental Research Funds for the Central Universities（2018CDYJSY0055) and CSC scholarship. GYW appreciated the financial support from the Key Research Program for Frontier Sciences, CAS under the award No. QYZDB-SSW-SLH016. The work by FZ was performed under the auspices of the US DOE by Lawrence Livermore National Laboratory under Contract DE-AC52-07NA27344. YX and VO were supported by the US Department of Energy, Office of Science, Basic Energy Sciences under grant No. DE-FG02-07ER46433. This research used resources of the National Energy Research Scientific Computing Center, a DOE Office of Science User Facility supported by the Office of Science of the US Department of Energy under Contract No.DE-AC02-05CH11231.

References

1 L. E. Bell, *Science,* 2008, **321**, 1457-1461.
2 G. J. Snyder, E. S. Toberer, *Nat. Mater.,* 2008, **7**, 101-110.
3 G. D. Mahan, *Solid State Phys.,*1998, **51**.
4 J. Wang, O. I. Lebedev, K. Lee, J.-A. Dolyniuk, P. Klavins, S. Bux, K. Kovnir, *Chem. Sci.,* 2017, **8**, 8030-8038.
5 V. Ponnambalam, S. Lindsey, W. Xie, D. Thompson, F. Drymiotis, T. M. Tritt, *J. Phys. D. Appl. Phys.,* 2011, **44**, 155406.
6 V. Ponnambalam, D.T. Morelli, *J. Electron. Mater.,* 2014, 43, 1875-1880.
7 G. D. Mahan, J. O. Sofo, *P. Natl. Acad. Sci.,* 1996, **93**, 7436-7439.
8 L. D. Hicks, M. S. Dresselhaus, *Phys. Rev. B,* 1993, **47**, 12727.
9 D. M. Rowe, V. L. Kuznetsov, L. A. Kuznetsova, *J. Phys. D. Appl. Phys.,* 2002, 35, 2183.
10 D. Parker, X. Chen, and D. J. Singh, *Phys. Rev. Lett.,* 2013, **110**, 146601.
11 D. Parker, A. May, and D. J. Singh, *Phys. Rev. Applied,* 2015, **3**, 064003.
12 D. I. Bilc, G. Hautier, D. Waroquiers, G. M. Rignanese, P. Ghosez, *Phys. Rev. Lett.,* 2015, **114**, 136601.
13 J. Nuss, U. Wedig, W. J. Xie, P. Yordanov, J. Bruin, R. Hubner, A. Weidenkafft, H.Takagi, *Chem. Mater.,* 2017, **29**, 6956-6965.
14 J. D. Comins, C. Heremans, M. D. Salleh, G. A. Saunders, W. Honle, *J. Mater. Sci. Lett.,*1986, **5**, 1195-1197.
15 P. E. Blochl, *Phys. Rev. B,* 1994, **50**, 17953.
16 G. Kresse, J. Furthmuller, *Comp. Mater. Sci.,*1996, **6**, 15-50.
17 G. Kresse, D. Joubert, *Phys. Rev. B,* 1999, **59**, 1758.
18 J. P. Perdew, K. Burke, M.Ernzerh, *Phys. Rev. Lett.,* 1996, **77**, 3865.
19 J. P. Perdew, A. Ruzsinszky, G. I. Csonka, O. A.Vydrov, G. E. Scuseria, L. A. Constantin, X. L. Zhou, K. Burke, *Phys. Rev. Lett.,* 2008, **13**, 136406.
20 F. Zhou, W. Nielson, Y. Xia, V. Ozolins, *Phys. Rev. Lett.,* 2014, **113**, 185501.
21 W. Li, J. Carrete, N. A. Katcho, N. Mingo, *Comput. Phys. Commun.,* 2014, **185**, 1747-1758.
22 X. Lu, D. T. Morelli, Y. Xia, F. Zhou, V. Ozolins, H. Chi, X. Y. Zhou, C. Uher, *Adv. Energy Mater.,* 2013, **3**, 342-348.
23 K. Suekuni, K. Tsuruta, T. Ariga, M. Koyano, *Appl. P*hys. *Express,* 2012, 5, 051201.
24 W. Lai, Y. X. Wang, D. T. Morelli, X. Lu, *Adv. Funct. Mater.,* 2015, **25**, 3648-3657.
25 Y. Bouyrie, C. Candolfi, S. Pailhes, M. M. Koza, B. Malaman, A. Dauscher, J. Tobolab, O. Boisron, L. Saviot, B. Lenoir, *Phys. Chem.Chem. Phys.,* 2015, **17**, 19751-19758.
26 W. Kevin Kuhn, Silver Gallium Sulfide by XPS, *Surf. Sci. Spect.,* 1994, **3**, 100-104.
27 H. Z. Zhao, J. E. Sui, Z. J. Tang, Y. C. Lan, Jie, J. Qing, D. Kraemer, K. N. McEnaney, A. Guloy, G. Chen, Z. F. Ren, *Nano Energy* 2014, **7**, 97-103.
28 H. Liu, X. Shi, F. Xu,; L. Zhang,; W. Zhang, L. Chen, Q. Li, C. Uher, T. Day, G. J. Snyder, *Nat. Mater.* 2012, **11**, 422-425
29 L.D. Zhao,; S.-H. Lo, Y. Zhang, H. Sun, G. Tan, C. Uher, C. Wolverton, V. P. Dravid, M. G. Kanatzidis, *Nature* 2014, **508**, 373-377
30 Y. He, T. Day, T. Zhang, H. Liu, X. Shi, L. Chen, G.J. Snyder, *Adv. Mater.* 2014, **26**, 3974-3978
31 G.Tan, F. Shi, S. Hao, H. Chi, L. D. Zhao, C. Uher, C. Wolverton, V. P. Dravid, M. G. Kanatzidis, *J. Am. Chem. Soc.* 2015, **137**, 5100-5112.
32 Y. Lee,; S.H. Lo, C. Chen, H. Sun,; D.-Y. Chung, T. C. Chasapis, C. Uher, V. P. Dravid, M. G. Kanatzidis, *Nat. Commun.* 2014, **5**, 3640.

33 D. W. Bullett, G. P. Witchlow , *Phys. Rev. B,*1986, **33**, 2429.
34 K, Köhler, H. J. Queisser, W. Hönle, G. Vonschnering, M. C. Bohm, *Physical Review B,* **31**, 6514.
35 C. S. Wang, W. E. Pickett, *Phys. Rev. Lett.,*1983, **51**, 597.
36 Y. Z. Pei, A. LaLonde, H. Wang, L. D. Chen, G. J. Snyder, *Nature,* 2011, **473**, 66.
37Y. L. Tang, Z. M. Gibbs, L. A. Agapito, G. Li, H. S. Kim, M. B. Nardelli, S. Curtarolo, G. J. Snyder, *Nat. Mater.,* 2015, **14**, 1223.
38 Y. Z. Pei, H. Wang, G. J. Snyder, *Adv. Mater.,* 2012, **24**, 6125-6135.
39 C. Linke, M. Jansen, *Inorg. Chem.* 1994, **33**, 2614-2616.
40 J. Wang, K. Lee, K. Kovnir, *Inorg. Chem.* 2016, **56**, 783-790.
41 J. E. Turney, E. S. Landry, A. J. H. McGaughey, C. H. Amon, *Phys. Rev. B*, 2009, **79**, 064301.

An alternative strategy to create optimum band shape for superior thermoelectric transport performance by utilizing stereochemically active lone pair s electrons is purposed, which has been demonstrated in the hole-doped phosphide compounds $Ag_6Ge_{10(1-x)}Ga_{10x}P_{12}$.